Synchronization principles of gamma rhythms in monkey visual cortex

Authors: E.Lowet[1]*, M.J.Roberts[1], A.Peter[2], B.Gips[3], P.De Weerd[1]

Affiliations:

[1] Psychology and Neuroscience, Maastricht University, Maastricht, The Netherlands

[2] Ernst Strüngmann Institute (ESI) for Neuroscience in Cooperation with Max Planck Society, Frankfurt, Germany

[3] Donders Institute for Brain, Cognition and Behaviour, Radboud University Nijmegen, Nijmegen, The Netherlands

*Correspondence to: eric.lowet@maastrichtuniversity.nl

Neural synchronization[1–5] in the gamma-band (25-80Hz) can enhance and route information flow during sensory[6–8] and cognitive processing[2,9–11]. However, it is not understood how synchronization between neural groups is robustly achieved and regulated despite of large variability in the precise oscillation frequency[10,12–16]. A common belief is that continuous frequency matching over time is required for synchronization and that thus rhythms with different frequencies cannot establish preferred phase-relations. Here, by studying gamma rhythms in monkey visual area V1, we found that the temporal variation of the frequency difference was to the contrary essential for synchronization. Gamma rhythms synchronized by continuously varying their frequency difference in a phase-dependent manner. The synchronization level and the preferred phase-relation were determined by the amplitude and the mean of the frequency difference variations. Strikingly, stronger variation of the frequency difference led to stronger synchronization. These observations were reproduced by a biophysical model of gamma rhythms[8,17–19] and were explained within the theory of weakly coupled oscillators[20–25]. Using a single and general equation, we derived analytical predictions that precisely matched our V1 gamma data across different stimulus conditions. Our work reveals the principles of how gamma rhythms synchronize, where phase-dependent frequency variations play a central role. These frequency variations are characteristic for the intermittent synchronization regime, a non-stationary regime naturally occurring between the states of complete synchrony and asynchrony. This regime allows for synchronization between rhythms of variable frequencies, which is essential for achieving robust synchronization in the complex and noisy networks of the brain.

To study the principles of neural synchronization we developed an experimental approach using V1 gamma oscillations. V1 gamma is subject to excellent experimental control, as it emerges locally and retinotopically, with a preferred oscillation frequency that can be readily manipulated by stimulus input properties[14,16]. Further, its generative mechanism is one of the best understood in the brain[26,2]. We first asked how synchronization within V1 was influenced by frequency differences, and by distance between recording sites. To this aim, we recorded from 2 to 3 laminar probes simultaneously in cortical area V1 of two macaques (M1 and M2) (Fig.1A). We investigated distances on the order of magnitude of V1 horizontal connectivity[27] hence probes were separated by between 1 and 6mm. Using laminar probes enabled us to reduce volume conduction by calculating current-source density (CSD) as a network signal. Using CSD, we estimated the instantaneous frequency, phase and phase difference of gamma signals. The monkeys fixated centrally while a whole-field static grating was shown with spatially variable contrast. Gamma power was induced in layers 2-4 and in the deepest layer (Fig.1B, Fig.S2). V1 locations showed increased gamma frequency with increased local contrast (Fig.1C). The frequency difference correlated with a difference in the MUA spike rate between probes (Fig.S4). Correspondingly, neurons recorded from different probes, in whose receptive fields (RFs) different contrasts were placed, showed different mean gamma frequencies (linear regression, single contact level, M1: R^2=0.31, M2: R^2= 0.25, both $p<10^{-10}$), giving us control to parametrically vary the frequency difference between probes.

We will first show the key results through three illustrative examples. In the first example, we chose two cortical locations separated by a relatively large distance of ~5mm, presented with a visual contrast difference of 17% (Fig.1D). Their frequency difference was 5Hz as shown by their non-overlapping power spectra (Fig.1E). This would imply that the phase difference would not be constant, but would advance at a phase precession rate of 2π every 200ms, which could be expected to preclude synchronization. However, the frequency difference was not constant. Instead, the instantaneous frequency difference was modulated as a function of phase difference (Fig.1F) with a modulation amplitude of 1Hz. At the smallest frequency difference (4Hz, yellow point) the phase precession was slowest, at 2π every 250ms, meaning that the oscillators stayed relatively longer around that phase difference. As a result, the probability distribution of phase differences over time (Fig.1G) was non-uniform giving a phase-locking value[28] (PLV) of 0.11. The peak of the distribution, the 'preferred phase', was at 1.3rad, in line with the minimum of the instantaneous frequency modulation function. In the second example, we chose a pair with a similar frequency difference of 4.8Hz and a closer distance (~2.5mm, Fig.1H). The instantaneous frequency modulation amplitude was larger with 1.8Hz modulation amplitude (Fig.1J) with a modulation minimum around 3Hz at the preferred phase. Because phase precession at the preferred phase was slower, the phase difference distribution was narrower indicating higher synchrony (PLV=0.32, Fig.1K) with a peak centered at a different phase (0.78rad). In the third example the cortical distance remained the same and the frequency difference was reduced (2.8Hz) by eliminating the contrast difference (Fig.1M, the remaining frequency difference might be due eccentricity, see Fig.S4). The frequency modulation amplitude did not change

however, with a lower mean difference, the modulation minimum was close to zero (1Hz, Fig.1N), thus the associated phase difference (0.48rad) could be maintained for relatively longer periods and the phase difference probability distribution was even narrower (PLV=0.51, Fig.1O). The three examples were representative for the 1079 recorded contact pairs in monkey M1 and 887 contact pairs in monkey M2.

We now show how the observed behavior can be accounted for within the mathematical framework of the theory of weakly coupled oscillators[20–25], where V1 populations can be approximated as oscillators, 'weakly coupled' by horizontal connections. According to the theory, the synchronization of two coupled oscillators can be predicted from the forces they exert on each other as a function of their instantaneous phase difference. This interaction function is referred to as the phase-response curve (PRC). Accordingly, the phase precession of two given cortical V1 locations is reduced to:

$$(1)\quad \dot{\theta} = \Delta\omega + \varepsilon G(\theta) + \eta$$

where $\dot{\theta}$ is the time derivative of the phase difference θ (the rate of phase precession), $\Delta\omega$ the detuning (the frequency difference), ε the interaction strength, $G(\theta)$ is defined as the mutual PRC, and η the phase noise, where $\eta \sim N(0,\sigma)$. Phase noise is here defined as variation, unrelated to interaction, that likely occurs for neural oscillators due to inherent instabilities of the generation mechanism[13,12] and due to other complex interactions occurring in cortical networks. For convenience, we express ω, ε and η in units of Hz (1Hz=2π*rad/s). The time derivative $\dot{\theta}$ is also expressed in Hz (instantaneous frequency, IF). Equation 1 was solved analytically to study changes in the phase-difference probability distribution, here characterized by the PLV and the mean (preferred) phase difference, as a function of detuning $\Delta\omega$ and interaction strength ε.

The theory predicts that the PLV and the mean phase difference result from an interplay between the detuning and interaction strength (Fig.S1). When detuning is smaller than the interaction strength ($\Delta\omega<\varepsilon$), the PLV is high and the mean phase difference is small. When detuning is larger than the interaction strength ($\Delta\omega>\varepsilon$), the PLV is low and the mean phase difference is large. With stronger interaction strength ε, larger detuning $\Delta\omega$ can be 'tolerated', leading to a triangular shaped region of high PLV in the $\Delta\omega$ - ε space termed the "Arnold tongue"[21,24,29]. Oscillators start to phase precess due to detuning or due to destabilization by phase noise[24]. Oscillators show linear phase precession if uncoupled. If coupled, the phase precession is non-linear and modulated by phase difference through the PRC, leading to instantaneous frequency modulations ($\Delta IF(\theta)$); a regime called intermittent synchronization[24,30,31,29]. In this regime, there is a preferred phase difference at which the instantaneous frequency difference is minimized.

The power of using the theory is the possibility to make precise predictions of the PLV and mean phase difference as a function of $\Delta\omega$ and ε. According to equation 1, the time-averaged modulation of the instantaneous frequency difference by phase difference, $\Delta\overline{IF}(\theta)$ (Fig.1F,J,N), directly relates to the deterministic term $\Delta\omega+\varepsilon G(\theta)$, as noise is averaged out. We used the

observed $\Delta\overline{IF}(\theta)$ to estimate the underlying synchronization properties. We estimated a single $G(\theta)$ function and σ value for a given whole dataset assuming stability of underlying PRCs and of the noise sources, whereas $\Delta\omega$ and ε was estimated for each contact pair and condition. Specifically, the $G(\theta)$ was estimated by the modulation shape of the $\Delta\overline{IF}(\theta)$ put to unity (see supplementary materials). We estimated interaction strength ε by the modulation amplitude of their $\Delta\overline{IF}(\theta)$ and detuning $\Delta\omega$ by the average value of their $\Delta\overline{IF}(\theta)$ computed over $[-\pi\ \pi]$. The remaining parameter σ was approximated by finding the σ value for equation 1 that could reproduce the observed overall instantaneous frequency variability (full description the theory of weakly coupled oscillators and parameter estimation in supplementary materials).

Before addressing whether the theory captures V1 gamma synchronization, we first tested our approach in a computational model of gamma oscillations in which the underlying network parameters were known. To that aim, we investigated simulations of two coupled Pyramidal-Interneuron gamma (PING) spiking networks[8,17–19] (Fig.2A). The gamma frequency was modulated by input drive[17,18,32] (R^2=0.98, Fig.2B), whereas the interaction strength ε was modulated by inter-network synaptic connectivity strength (R^2=0.97, green arrows, Fig.2A). For each network we estimated a population signal from which we extracted their instantaneous phase difference (Fig.2C). By reconstructing the $G(\theta)$ (see example of $\Delta\overline{IF}(\theta)$ in Fig.2D) and estimating phase noise variance (σ=15Hz), we could solve equation 1 and we found that the theory (Fig.2F-I) accurately predicted the PLV (model accuracy: R^2=0.93) and the mean phase difference (model accuracy: R^2= 0.94). Mapping the gamma PLV and the mean phase difference in the $\Delta\omega$ - ε parameter space yielded the predicted Arnold tongue.

We then tested whether the theory predicted the in vivo data with equal success. In the same manner as with PING modeling data, we estimated for each monkey the $G(\theta)$ (see representative $\Delta\overline{IF}(\theta)$ examples in Fig.3A and F) and the phase noise variance (M1:σ=19Hz, M2:σ=20Hz). The interaction strength ε was found to be inversely correlated to the cortical distance between probes (M1: R^2=0.41, M2: R^2=0.29, both $p < 10^{-10}$, Fig.S5E) in line with anatomy of horizontal connectivity[27]. Quantitative predictions were derived of V1 gamma synchronization for different $\Delta\omega$ and ε values. We found that gamma PLV closely followed the analytical predictions as a function of $\Delta\omega$ and ε (model accuracy for population averages: M1: R^2=0.88, M2: R^2= 0.90; for single contact data: M1: R^2=0.18, M2: R^2= 0.32, see in Fig.3B/G). The PLV was dependent on both interaction strength ε and detuning $\Delta\omega$ (Fig.S7), and showed the predicted Arnold tongue in both M1 and M2 (Fig.3C/H). The mean phase differences (dots in Fig.3D/I) were also well predicted by the analytical model as a function of $\Delta\omega$ and ε (gray line; model accuracy for population averages: M1: R^2=0.94, M2: R^2=0.88, for single-contact data: M1: R^2=0.56, M2: R^2=0.27). The phase difference was largely determined by detuning $\Delta\omega$ and more weakly by interaction strength ε (Fig.S7). The phase spread (Fig.3E/J) had a range of nearly –pi/2 to pi/2 in both M1 and M2 as predicted by the shape of $G(\theta)$ (Fig.S1). We confirmed the phase locking value and phase difference analysis in spike-CSD and spike-spike measurements (Fig.S8).

The present study shows that gamma synchronization in PING networks and in awake monkey V1 adheres to theoretical principles of weakly coupled oscillators[20–25], thereby providing insight into the dynamic principles underlying neural synchronization. Crucially, we observed phase-dependent modulations of the instantaneous frequency difference in both PING model and V1 recording data. These modulations are characteristic for the intermittent synchronization regime[24,29–31] which naturally arises in frequency-variable and noisy oscillator networks.. These observations show that a fixed and common frequency is not per se required for synchronization[10,14]. To the contrary, these non-stationary frequency modulations reflect the essential process of synchronization and, furthermore, allow the experimental estimation of the interaction function[20–25] and of the regulative parameters underlying gamma synchronization. We found that two parameters mainly regulated synchronization: the detuning $\Delta\omega$ (mean frequency difference) and the interaction strength ε (amplitude of frequency modulations). This was highlighted in the mapping of the Arnold tongue[21,24,29], a predicted synchronization region within the parameter space of detuning and interaction strength. In our experiment, detuning was dependent on the local contrast difference[14,16], known to change neural excitation in V1[33], while the interaction strength was dependent on the underlying horizontal connectivity strength, here varied by cortical distance[27]. These properties suggest V1 gamma as a relevant mechanism for sensory processing[6,7] as local gamma synchronization will be informative about the sensory input[8] and informative about the underlying structure of connectivity. Gamma frequency is indeed modulated by various sensory stimuli[2,14,16,15,34] and by cognitive manipulations[26,2,10]. Importantly, in line with previous findings[14,35–37], we found V1 gamma synchrony to be local, restricted by horizontal connectivity that extends only few mm across the cortex[27], and hence not likely to reflect whole perceptual objects. Our findings reconcile several studies that have given different theoretical interpretations to observations of frequency variation in gamma[14,16,12], and are relevant for understanding synchronization with and across cortical areas where differences in preferred frequency were also observed[9,10]. Given the generality of the observed synchronization principles, they are likely to apply to other brain regions and frequency bands.

Methods summary:

Experimental recording: We recorded in two adult male rhesus monkeys, implanted with a chamber above early visual cortex, positioned over V1/V2. A head post was implanted to head-fix the monkeys during the experiment. The monkey´s task was to passively gaze on a fixation point while a whole-field static square-wave grating was shown. We simultaneously recorded from multiple locations in monkey V1 while the monkey viewed luminance gratings in which spatially varying contrast set the frequencies of local gamma rhythms[14,16]. V1 recordings were made with 16-contact laminar Plexon U-probes (Plexon Inc.). We recorded the local field potential (LFP) and multi-unit spiking activity (MUA). We aligned the neural data from the different laminar probes according to their cortical depth and excluded contacts coming from

deep V2. All the procedures were in accordance with the European council directive 2010/63/**EU**, the Dutch 'experiments on animal acts' (1997) and approved by the Radboud University ethical committee on experiments with animals (Dier-Experimenten-Commissie, DEC).

Theoretical and computational modelling: Using the formulism of the theory of weakly coupled oscillators we investigated the phase-locking as well as the mean phase difference of two mutually coupled noisy phase-oscillators with variable intrinsic frequency difference (detuning) and interaction strength. The stochastic differential equation was solved analytically[24]. The analytical results correctly predicted the numerical simulations. In addition, we simulated two coupled excitatory-inhibitory spiking networks generating gamma oscillations using Izhikevich-type neuronal model. The detuning between the networks was altered by changing the difference in excitatory input drive. The interaction strength was altered by changing the cross-network synaptic connection strength.

Signal analysis and statistics: To investigate dynamical changes in the gamma phase and frequency over time we estimated the instantaneous gamma phase and frequency using the singular spectrum decomposition of the signal (SSD, see https://project.dke.maastrichtuniversity.nl/ssd/). The accuracy of the theoretical predictions for the experimental data was quantified as the explained variance R^2. We also used a multiple regression approach to quantify the dependence of synchronization on amplitude, detuning and interaction strength. Full methods and additional supportive results are provided in the *Supplementary Information*.

References:

1. Buzsáki, G., Anastassiou, C. A. & Koch, C. The origin of extracellular fields and currents--EEG, ECoG, LFP and spikes. *Nat. Rev. Neurosci.* **13,** 407–20 (2012).
2. Fries, P. Rhythms For Cognition: Communication Through Coherence. *Neuron* (2015).
3. Maris, E., Fries, P. & van Ede, F. Diverse Phase Relations among Neuronal Rhythms and Their Potential Function. *Trends Neurosci.* **39,** 86–99 (2016).
4. Buehlmann, A. & Deco, G. Optimal information transfer in the cortex through synchronization. *PLoS Comput. Biol.* **6,** (2010).
5. Womelsdorf, T. *et al.* Modulation of neuronal interactions through neuronal synchronization. *Science* **316,** 1609–1612 (2007).
6. Gray, C. M. & Singer, W. Stimulus-specific neuronal oscillations in orientation columns of cat visual cortex. *Proc. Natl. Acad. Sci. U. S. A.* **86,** 1698–702 (1989).
7. Eckhorn, R. *et al.* Flexible cortical gamma-band correlations suggest neural principles of visual processing. *Vis. cogn.* **8,** 519–530 (2001).
8. Besserve, M., Lowe, S. C., Logothetis, N. K., Schoelkopf, B. & Panzeri, S. Shifts of Gamma Phase across Primary Visual Cortical Sites Reflect Dynamic Stimulus-Modulated Information Transfer. *PLoS Biol.* **13,** (2015).
9. Gregoriou, G. G., Gotts, S. J., Zhou, H. & Desimone, R. High-frequency, long-range coupling

between prefrontal and visual cortex during attention. *Science* **324,** 1207–1210 (2009).
10. Bosman, C. A. *et al.* Attentional stimulus selection through selective synchronization between monkey visual areas. *Neuron* **75,** 875–888 (2012).
11. Kim, H., Ährlund-Richter, S., Wang, X., Deisseroth, K. & Carlén, M. Prefrontal Parvalbumin Neurons in Control of Attention. *Cell* **164,** 208–218 (2016).
12. Burns, S. P., Xing, D., Shelley, M. J. & Shapley, R. M. Searching for autocoherence in the cortical network with a time-frequency analysis of the local field potential. *J Neurosci* **30,** 4033–4047 (2010).
13. Atallah, B. V & Scanziani, M. Instantaneous modulation of gamma oscillation frequency by balancing excitation with inhibition. *Neuron* **62,** 566–577 (2009).
14. Ray, S. & Maunsell, J. H. R. Differences in gamma frequencies across visual cortex restrict their possible use in computation. *Neuron* **67,** 885–96 (2010).
15. Jia, X., Xing, D. & Kohn, A. No consistent relationship between gamma power and peak frequency in macaque primary visual cortex. *J Neurosci* **33,** 17–25 (2013).
16. Roberts, M. J. *et al.* Robust gamma coherence between macaque V1 and V2 by dynamic frequency matching. *Neuron* **78,** 523–36 (2013).
17. Tiesinga, P. H. & Sejnowski, T. J. Mechanisms for Phase Shifting in Cortical Networks and their Role in Communication through Coherence. *Front Hum Neurosci* **4,** 196 (2010).
18. Lowet, E. *et al.* Input-Dependent Frequency Modulation of Cortical Gamma Oscillations Shapes Spatial Synchronization and Enables Phase Coding. *PLoS Comput. Biol.* **11,** e1004072 (2015).
19. Cannon, J. *et al.* Neurosystems: brain rhythms and cognitive processing. *Eur. J. Neurosci.* **39,** 705–19 (2014).
20. Ermentrout, G. B. & Kleinfeld, D. Traveling electrical waves in cortex: insights from phase dynamics and speculation on a computational role. *Neuron* **29,** 33–44 (2001).
21. Kopell, N. & Ermentrout, G. B. Chapter 1 Mechanisms of phase-locking and frequency control in pairs of coupled neural oscillators. *Handb. Dyn. Syst.* **2,** 3–54 (2002).
22. Hoppensteadt, F. C. & Izhikevich, E. M. Thalamo-cortical interactions modeled by weakly connected oscillators: could the brain use FM radio principles? *Biosystems* **48,** 85–94 (1998).
23. Winfree, A. T. Biological rhythms and the behavior of populations of coupled oscillators. *J. Theor. Biol.* **16,** 15–42 (1967).
24. Pikovsky, A., Rosenblum, M., Kurths, J. & Hilborn, R. C. Synchronization: A Universal Concept in Nonlinear Science. *Am. J. Phys.* **70,** 655 (2002).
25. Kuramoto, Y. Collective synchronization of pulse-coupled oscillators and excitable units. *Phys. D Nonlinear Phenom.* **50,** 15–30 (1991).
26. Buzsáki, G. & Wang, X.-J. Mechanisms of gamma oscillations. *Annu Rev Neurosci* **35,** 203–225 (2012).
27. Stettler, D. D., Das, A., Bennett, J. & Gilbert, C. D. Lateral Connectivity and Contextual Interactions in Macaque Primary Visual Cortex. *Neuron* **36,** 739–750 (2002).
28. Lachaux, J. P., Rodriguez, E., Martinerie, J. & Varela, F. J. Measuring phase synchrony in brain signals. *Hum Brain Mapp* **8,** 194–208 (1999).
29. Izhikevich, E. M. *Dynamical Systems in Neuroscience: The Geometry of Excitability and Bursting*. *Dyn. Syst.* **25,** (2007).
30. Kozma, R. & Freeman, W. J. Intermittent spatio-temporal desynchronization and sequenced synchrony in ECoG signals. *Chaos An Interdiscip. J. Nonlinear Sci.* **18,** 037131 (2008).
31. Lowet, E., Roberts, M. J., Bonizzi, P., Karel, J. & De Weerd, P. Quantifying Neural Oscillatory Synchronization: A Comparison between Spectral Coherence and Phase-Locking Value Approaches. *PLoS One* **11,** e0146443 (2016).
32. Sancristóbal, B., Vicente, R. & Garcia-Ojalvo, J. Role of frequency mismatch in neuronal communication through coherence. *J. Comput. Neurosci.* **37,** 193–208 (2014).
33. Sclar, G., Maunsell, J. H. & Lennie, P. Coding of image contrast in central visual pathways of the

macaque monkey. *Vision Res.* **30,** 1–10 (1990).
34. Feng, W., Havenith, M. N., Wang, P., Singer, W. & Nikolić, D. Frequencies of gamma/beta oscillations are stably tuned to stimulus properties. *Neuroreport* **21,** 680–4 (2010).
35. Palanca, B. J. A. & DeAngelis, G. C. Does neuronal synchrony underlie visual feature grouping? *Neuron* **46,** 333–46 (2005).
36. Gail, A., Brinksmeyer, H. J. & Eckhorn, R. Contour decouples gamma activity across texture representation in monkey striate cortex. *Cereb Cortex* **10,** 840–850 (2000).
37. Jia, X., Smith, M. A. & Kohn, A. Stimulus Selectivity and Spatial Coherence of Gamma Components of the Local Field Potential. *J. Neurosci.* **31,** 9390–9403 (2011).

Acknowledgments: We thank N.Kopell, W.Singer, A.Bastos, P.Fries, C.Micheli, F.Smulders, J.v.d.Eerden, J.Karel, P.Bonizzi, A.Hadjipapas, A.A.v.d.Berg. Supported by NWO VICI grant 453-04-002 to PDW and NWO VENI grant 451-09-025 to MJR. All data are stored at the Department of Psychology and Neuroscience, Maastricht University, The Netherlands. We thank the Radboud University Nijmegen for hosting our experiments, and staff of the Central Animal Facility (CDL) for expert assistance.

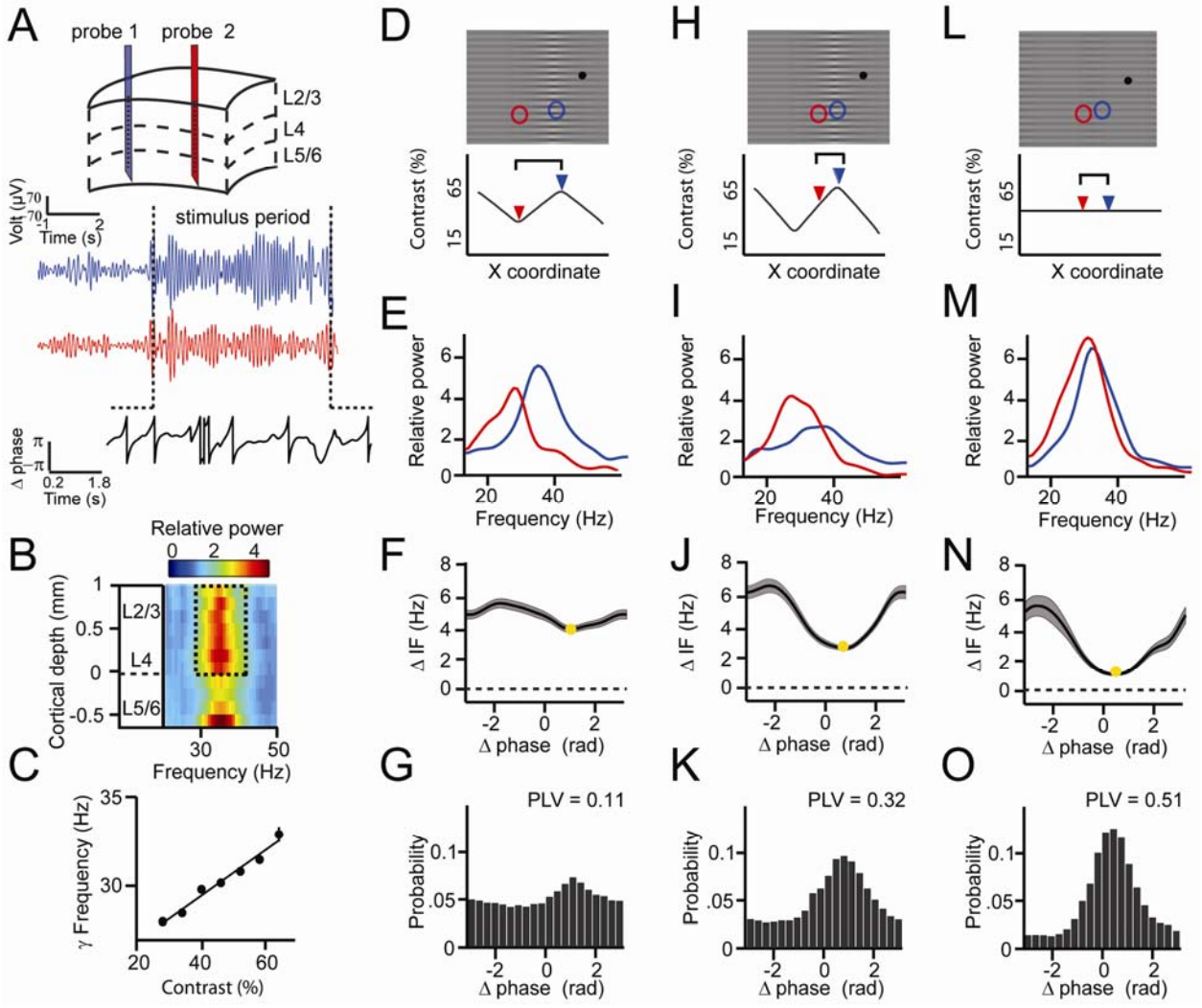

Fig.1. Experimental paradigm and intermittent synchronization. **(A)** Recordings preparation and example CSD (blue and red) traces from which phase difference (black) trace was extracted. The gradient of the black trace indicates the rate of phase precession. **(B)** Spectral power relative to baseline as a function of V1 cortical depth (36.5% contrast, population average, M1) dashed box indicates gamma in the layers taken for main analysis **(C)** Local contrast modulated gamma frequency (population average, M1). **(D-G)** Example 1 showing synchronization despite frequency difference. **(D)** Stimulus grating and fixation spot (black dot). Two receptive fields (RF) from different probes are superimposed (blue and red circles). Below, black line gives contrast over space, arrowheads mark RF positions. **(E)** Power spectra of the two probes showing different peak frequencies. **(F)** Instantaneous frequency difference (ΔIF), equivalent to phase precession rate, as a function of phase difference. Yellow dot indicates the modulation minimum equivalent to preferred phase difference, shading is ±SE (**G)** The phase difference probability distribution and phase-locking value (PLV). **(H-K)** Example 2; probes were closer, gamma peak frequency difference was similar. Conventions as in D-G. **(L-O)** Example 3; same distance,

reduced frequency difference. Compare F, J, N RF distance determine IF modulation amplitude, gamma frequency difference determines preferred phase difference.

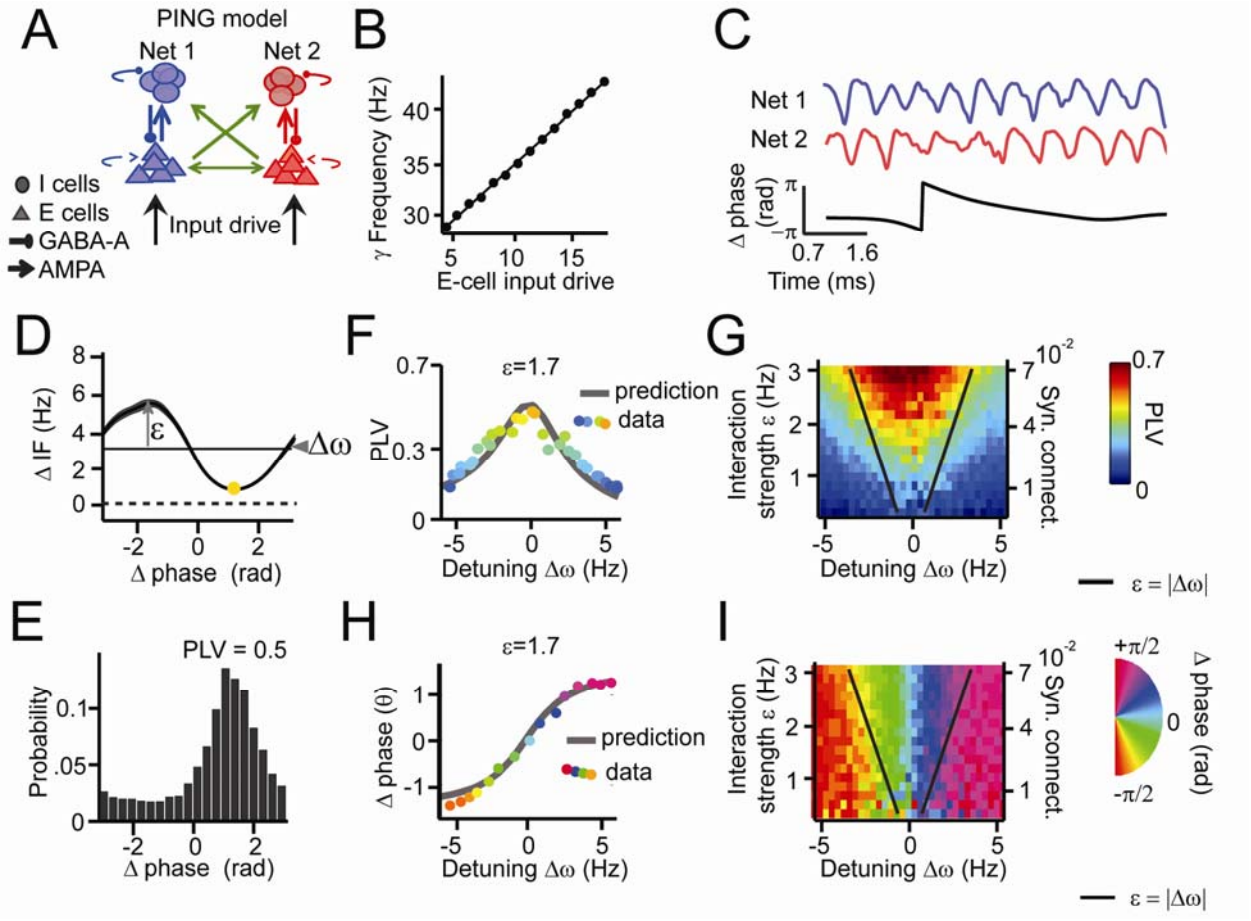

Fig.2. Applying the theory of weakly coupled oscillators to coupled PING networks. **(A)** Two coupled pyramidal-interneuron gamma (PING) networks (Net 1 and Net 2). **(B)** The frequency of gamma in a single network depends on input strength. **(C)** Simulation output example network signals (red and blue) and phase difference θ (black). **(D)** An example $\Delta\overline{\mathrm{IF}}(\theta)$ modulation used to estimate the interaction strength ε and detuning value Δω. The shape of the modulation indicates the G(θ). **(E)** The corresponding phase difference probability distribution. **(F)** The simulation PLV at different detuning values $\Delta\omega$ (dots colored by PLV) at a single interaction strength value (ε =1.7) was well predicted by the model (gray line). **(G)** The PLV at many interaction strengths and detuning values mapped the Arnold tongue. Black lines mark the predicted Arnold tongue borders in the noise-free case (ε=|$\Delta\omega$|). **(H-I)** As (F-G), but for preferred phase difference θ. Color code of dots in F and H as in G and I, respectively.

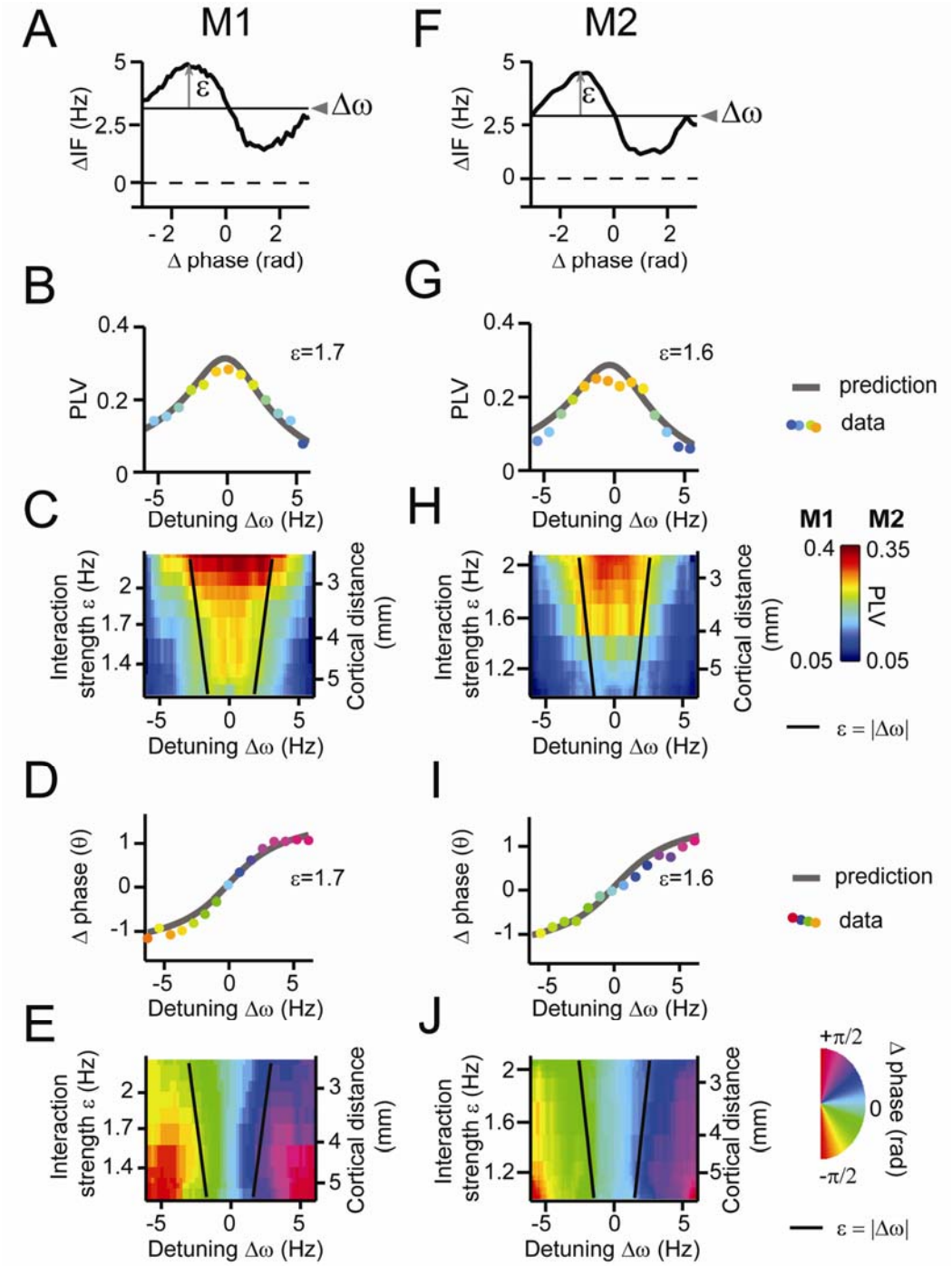

Fig.3.Predicting V1 gamma synchronization. **(A-E)** Results from M1. (**A)** An example $\Delta\overline{IF}(\theta)$ modulation used for estimating ε and Δω for monkey M1 (left) and M2 (right). The shape of the modulation indicates the G(θ). (**B)** Observed PLV (dots) and analytical prediction (gray line) as a

function of detuning $\Delta\omega$ for one level of interaction strength (ε=1.7). (**C)** Combining different detuning $\Delta\omega$ and interaction strengths ε we observed a triangular synchronization region, the Arnold tongue. Black lines mark the predicted Arnold tongue border as expected from the noise-free case ($\varepsilon=|\Delta\omega|$) (**D)** Analytical prediction (gray) and experimentally observed preferred phase differences (dots colored by phase difference) as a function of detuning $\Delta\omega$ for one level of interaction strength (ε=1.7). (**E)** Similar to C), but now plotting the preferred phase difference. **(F-J)** As (A-E) but for M2 population data. Color coding of dots in B, G, D, I is as indicated in color scales in panels just below them.